# HIGH EFFICIENCY GRAPHENE-SILICON HYBRID-INTEGRATED THERMAL AND ELECTRO-OPTICAL MODULATION: SUPPLEMENTAL DOCUMENT

## Supplementary Note 1 Graphene transfer and characterization

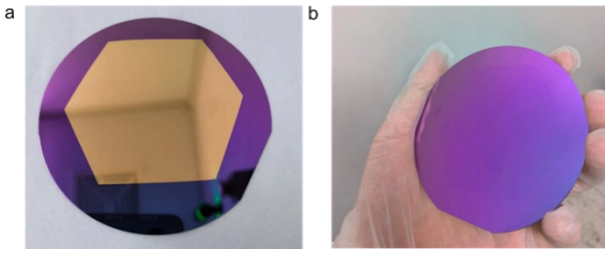


**Fig. S1. Gold-assisted transfer method. a,** Graphene-gold on a silicon wafer. **b,** Transparent graphene flake on a silicon wafer.

As indicated in the Fig. S1a, we employed the gold-assisted transfer method to transfer large-area hexagonal graphene flakes onto silicon substrates. Subsequently, we completely etched away the gold using acid. As depicted in Fig. S1b, the resulting graphene flakes exhibit intact and transparent characteristics, confirming the successful transfer process.

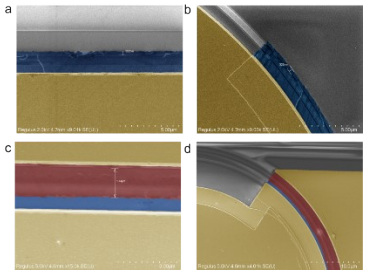


**Fig. S2. False-color SEM image of the device during the fabrication process. a-b,** The bottom SLG (blue) and gold (yellow). **c-d,** The bottom and the top SLG (blue and red) with gold (yellow) contacts.

Furthermore, we have provided some SEM images of the modulator fabrication process using the gold-assisted transfer method. Fig. S2a-b depict the transferred first layer of graphene-gold (the bottom), while Fig. S2c-d show images of the device after transferring the second layer of graphene-gold (the top).

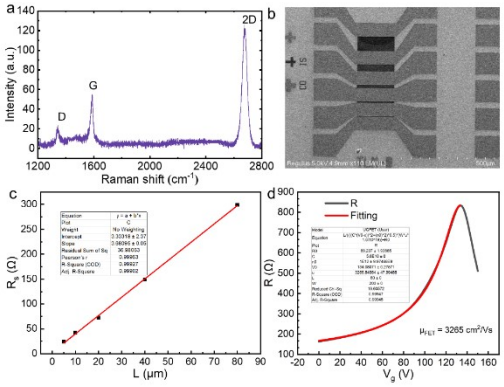


**Fig. S3. Graphene characterization. a,** Raman shift spectra of SLG. **b,** Graphene samples used for TLM testing. **c,** The measured surface resistance SLG and SLG-gold contact resistance. **d,** The mobility of SLG.

A typical Raman spectrum of the graphene on our devices is shown in Fig. S3a. Here we found that the 2D/G ratio is greater than two, which points to a cleaner surface with low doping level or contamination[1]. We attribute the presence of D peak to the impurities induced during the remove of copper substrate with ammonium persulfate and the growth of dielectric layer.

To characterize the electrical properties of graphene, we fabricated graphene samples, which were subsequently subjected to the transmission line method (TLM) measurement[2], as depicted in Fig. S3b. The graphene widths (L) in our samples were 5, 10, 20, 40, and 80 μm, with a constant graphene-metal contact length (W) of 200 μm. The test results illustrated in Fig. S3c indicate the measured surface resistance of single layer graphene (SLG) and SLG-gold contact resistance are 700 Ω/□ and 0.3 Ω·mm, respectively. In addition, we also fabricated graphene field-effect transistors (FETs) to assess the level of graphene mobility[3]. By fitting the experimental data (gray line) to appropriate models, as indicated by the red line in Fig. S3d, we determined the graphene mobility ($\mu_{FET}$) to be approximately 3265 $cm^2/Vs$.

These results indicate clean interface and low contact resistance for the gold-assisted transferred graphene, which is important in modulator performance improvement.

## Supplementary Note 2 Transmission spectra of the micro-ring resonator before and after fabricating graphene heater

The optical responses of the micro-ring resonator (MRR) before and after graphene heater integration were characterized by transmission measurements described in Methods. As shown in Fig. S2, the transmission spectrum of MRR after graphene heater fabrication (gray) shows a red-shift of 1.57 nm compared with bare MRR (green) due to the increased effective refractive index induced by the incorporation of graphene heater. The FSR of graphene integrated MRR remains unchanged and the insertion loss shows an increase of 4 dB.

The quality factor (Q) is denoted via $Q = \lambda_{res}/\Delta\lambda_{FWHM}$, where $\lambda_{res}$ is the selected resonance wavelength, and $\Delta\lambda_{FWHM}$ is the full width at half maximum (FWHM) of the corresponding resonance peak. And the Q values of bare MRR and graphene MRR are extracted to be 43000 and 67000 from the transmission spectrum. The observed increase in the Q value can be attributed to the transition from an overcoupled MRR without the graphene heater to a critically coupled MRR after the graphene heater fabrication.

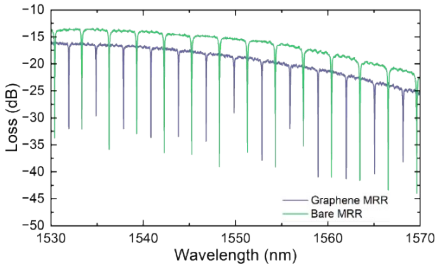


**Fig. S4. Transmission spectra before (green) and after (gray) incorporating the graphene heater.**

## Supplementary Note 3 The dependence of the effective refractive index in the active region on the applied bias voltage

The transmission light via the through port is expressed by equation (1)[4].

$$T = \left|\frac{b_1}{a_1}\right|^2 = \left|\frac{t - \alpha e^{j\theta}}{1 - \alpha t * e^{j\theta}}\right|^2 \quad (1)$$

Where, $t$ is the transmission factor, $\alpha$ is the linear loss and $\theta$ denotes the phase of light traveling in the ring, which is extracted by $\theta = \frac{2\pi}{\lambda} n_{eff} L$. We calculate the change in the effective refractive index ($\Delta n_{eff}$) of the propagating mode with different bias voltages from the shift of the resonance wavelength at 1552.86 nm. Since $\Delta n_{eff}$ is concentrated only in the length of the ring covered by Graphene, the change in phase can be derived as $\Delta\theta = \frac{2\pi}{\lambda} \Delta n_{eff_{Gra}} L_{Gra}$. In order to extract the change in the effective refractive index of active aera $\Delta n_{eff_{Gra}}$ from the transmission spectra, we track the evolution of the change in the resonance wavelength ($\Delta\lambda_{res}$) with voltage[5] and use equation (2).

$$m\left(\lambda_{res}(V) - \lambda_{res}(V = 0)\right) = \Delta n_{eff_{Gra}} L_{Gra} \quad (2)$$

Where, $m$ is the order of the micro-ring resonator, which is defined by $m = [n_{eff_{Si}} * L/\lambda_{res}(V = 0)]$ and $L = 2\pi R$, where R is the radius of the ring.

## Supplementary Note 4 I-V characteristic of the graphene TO modulator

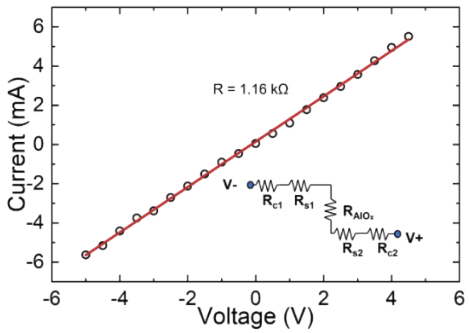


**Fig. S5. I-V characteristic of the graphene TO modulator.** Inset: the equivalent circuit of graphene TO modulator.

The total resistance of the proposed modulator includes three parts, i.e., the resistance of the dielectric $AlO_x$ $R_{AlOx}$, the total resistance of the graphene sheets $R_{sheets}$, and the total contact resistance between the graphene sheets and the Au electrodes $R_{contact}$, as shown in the inset of Fig. S3. Therefore, one has

$$R = R_{AlOx} + R_{sheets} + R_{contact} = \rho\frac{L_a}{dW_a} + R_s\frac{L_{g1}}{W_{g1}} + R_s\frac{L_{g2}}{W_{g2}} + \frac{R_c}{W_{c1}} + \frac{R_c}{W_{c2}}$$

where $R_s$ is the surface resistance of SLG, $R_c$ is the SLG-Au contact resistance. With the measured values of $R_s = 700\ \Omega/\square$ and $R_c = 300\ \Omega\cdot\mu m$, the resistances from the present device are $R_{sheets} = 179.8\ \Omega$ and $R_{contact} = 3.06\ \Omega$. Considering the total resistance $R = 1.16\ k\Omega$ extracted from I-V measurement (See Fig. S5), the resistivity of dielectric $AlO_x$ is estimated to be 194.81 $\Omega\cdot\mu m$.

## Supplementary Note 5 The equivalent circuit of the graphene EA modulator

The capacitance of the device presented in Fig. 4-5 of the main text is measure to be 200 fF.

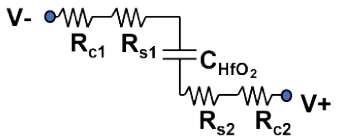


**Fig. S6. The equivalent circuit of the graphene EA modulator.**

## Supplementary Note 6 Measurement setup

For the static electro-optic response measurement, probes were employed to establish contact with electrodes and apply the static electrical signal from a source meter to the device under test (DUT) through gold electrodes. The input light in the TE mode from a tunable laser source was polarization controlled and then launched into the chip with a grating coupler. The output light is received by an optical power meter to collect the optical response. The tunable laser is scanned to obtain the spectra response.

For dynamic electro-optic response measurement, the source meter is replaced by a signal generator to apply a rectangular bias signal, and the modulated signal is detected by a photodetector and recorded by an oscilloscope to observe and analyze the device's behavior under varying input signals and time-dependent changes. The applied rectangular voltage was 1.85−2.15 V ($V_{pp}$ = 0.3 V) at a frequency of 50 kHz.

For small signal bandwidth measurement, the experimental setup involved the use of a bias tee to combine the DC signal (5 V) with the RF signal provided by a photonic network analyzer (PNA). This combined signal is then fed to the graphene EA modulator using a microwave probe. The signal light of a tunable laser source is amplified by an erbium-doped fiber amplifier (EDFA), polarization controlled by a PC before being modulated by the graphene EA modulator. The modulated light is amplified by another EDFA and further filtered using an optical tunable filter. Subsequently, the light was transmitted to a PNA for detection and analysis.

For eye diagram measurement, a $2^{15}-1$ pseudo-random binary sequence was generated using an arbitrary waveform generator driven by a 2 V peak-to-peak RF signal. This signal is amplified using a microwave amplifier and combined with the DC signal (5 V) by a bias tee. It is then fed to the graphene EA modulator using a microwave probe. The signal light of a tunable laser source is directly polarization controlled and then modulated, amplified and filtered. Finally, the output light is transmitted to an oscilloscope enabling the visualization and characterization of the modulated output waveform.

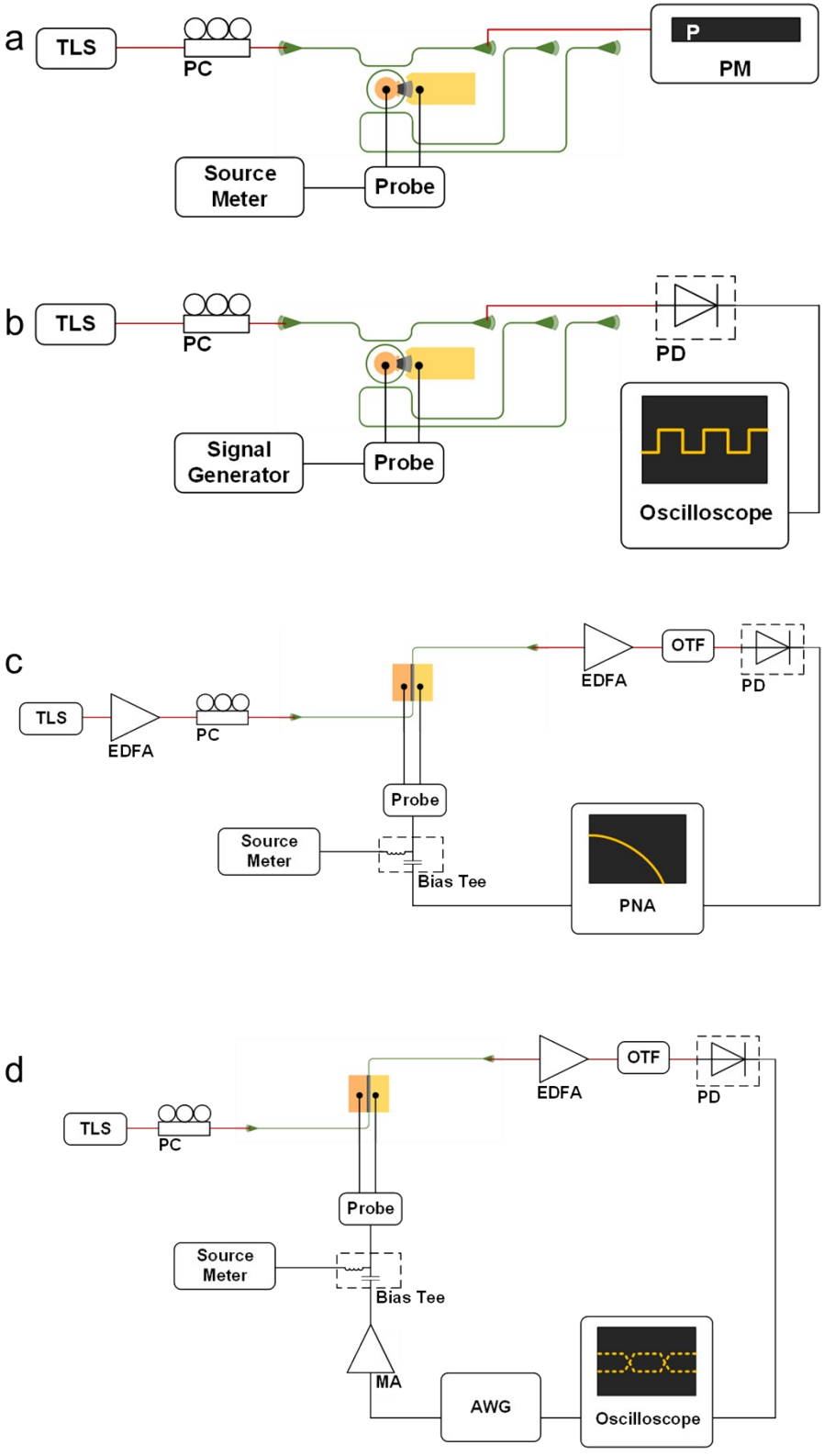


**Fig. S7. Experimental setup. a,** Static electro-optic response measurement. **b,** Dynamic electro-optic response measurement. **c,** Small signal bandwidth measurement. **d,** Eye diagram measurement. TLS: Tunable Laser Source, PC: Polarization Controller, PM: Power Meter. PD: Photodetector. EDFA: Erbium doped Fiber Amplifier. OTF: Optical Tunable Filter. PNA: Photonic Network Analyzer. AWG: Arbitrary Waveform Generator. MA: Microwave Amplifier.

## Supplementary Note 7 Eye diagram measurements

To validate the high-speed data transmission capabilities of the EA modulator, we measured the devices presented in Fig. 4 of the main text at different speeds. Figure S8 shows the eye diagrams of the non-return-to-zero (NRZ) signal of the graphene EA straight waveguide modulator.

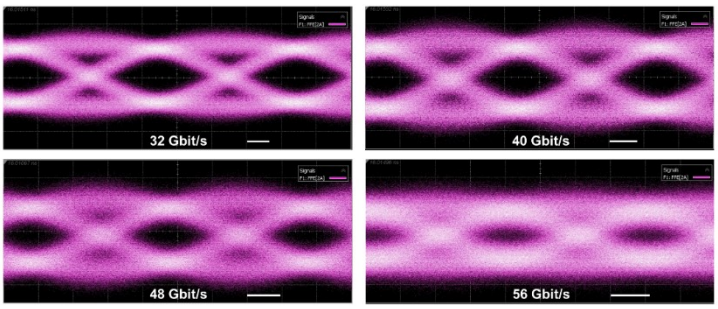


**Fig. S8. Eye diagrams of the device presented in Fig. 4 of the main text.** NRZ eye diagrams generated at data rates of 32, 40, 48 and 56 Gb/s. The white scale bar corresponds to 5 ps.

## REFERENCES

1 C. Casiraghi, S. Pisana, K. S. Novoselov, A. K. Geim and A. C. Ferrari, *Appl. Phys. Lett.*, 2007, **91**, 233108.

2 C. C. Lu, Y. C. Lin, C. H. Yeh, J. C. Huang and P. W. Chiu, *ACS Nano*, 2012, **6**, 4469–4474.

3 Y. Jia, X. Gong, P. Peng, Z. Wang, Z. Tian, L. Ren, Y. Fu and H. Zhang, *Nano-Micro Lett.*, 2016, **8**, 336–346.

4 A. Yariv, *Electron. Lett.*, 2000, **36**, 321.

5 I. Datta, S. H. Chae, G. R. Bhatt, M. A. Tadayon, B. Li, Y. Yu, C. Park, J. Park, L. Cao, D. N. Basov, J. Hone and M. Lipson, *Nat. Photonics*, 2020, **14**, 256–262.